Engineering Science and Technology, an International Journal 54 (2024) 101702

Contents lists available at ScienceDirect

Engineering Science and Technology, an International Journal

journal homepage: www.elsevier.com/locate/jestch

Full length article

Vibration data-driven anomaly detection in UAVs: A deep learning approach

Erkan Caner Ozkat

Recep Tayyip Erdogan University, Faculty of Engineering & Architecture, Department of Mechanical Engineering, Rize, 53100, Turkey

ARTICLE INFO

Keywords:
Unmanned Aerial Vehicles
Fault detection
Vibrations
Predictive maintenance
Deep learning

ABSTRACT

Unmanned Aerial Vehicles (UAVs) are employed for diverse applications, including aerial surveillance and package delivery. However, the occurrence of faults, especially propeller failures, poses significant risks to safe and efficient operations. Detecting such faults at an early stage is critical to avoiding catastrophic outcomes and ensuring the reliability and lifespan of UAVs. To address this crucial need, this study proposes a novel approach for monitoring vibration signals using a wavelet scattering long short-term memory (LSTM) autoencoder network. The LSTM autoencoder can learn temporal patterns from input signals, whereas wavelet scattering can capture the dynamics and interactions of various frequency components of signals. First, a deliberate modification was made to one of the propeller blades of the DJI M600 multi-rotor UAV to deliberately induce vibration. The proposed network was then evaluated on the acquired vibration signal using the MTi-G-700 IMU. The results showed that warning signals were generated from all axes before failures occurred. Notably, the earliest warnings were obtained from y-axis data within 100 s, while the first warning from z-axis data was recognized 130 s later. The failure occurred at roughly 280 s. The experimental findings indicate that the proposed method can accurately detect anomalies that could potentially lead to failure.

1. Introduction

Unmanned Aerial Vehicles (UAVs) have become increasingly popular in recent years for a variety of applications, including surveillance, delivery, and agriculture [1–3]. Despite their versatile applications, the safety and reliability of UAVs fall behind that of manned aircraft, largely due to the absence of real-time human observation and rapid decision-making capabilities. This underscores the pressing need for effective anomaly detection methods to enhance UAV safety. The most common faults in UAVs can be classified into three categories: structural [4,5], electrical [6,7], and communication faults [8,9]. The structural faults that occur during the flight have more critical importance than others for the safe and effective operation of UAVs because any problem might have severe consequences such as collisions or accidents [10,11]. It was revealed that 67% of UAV accidents were caused by failures in the mechanical system, and 53% of these failures occurred in the propulsion system, where the main components are the rotor and propeller [12,13]. UAVs can weigh up to 25 kg and move at speeds close to 45 m/s. Mechanical failures, which may manifest during the execution of tasks such as goods delivery or civil infrastructure inspection in residential areas, were reported to cause soft tissue injuries, eye loss, and severe lacerations [14]. In addition, UAVs cause other types of accidents, such as traffic accidents, due to distraction while flying at low altitudes for monitoring real-time traffic [15].

Structural failures often occur in components that have mechanical functions, such as rotors, propellers, and actuators, and these components are more prone to fail during flight [16,17]. This is due to the stress they are exposed to during flight, which causes them to wear out over time. In particular, rotors and propellers rotating at high speed increase the likelihood of encountering problems because minor faults can quickly turn into more serious problems. It is, therefore, essential to monitor the health of structural components to prevent failure during flight. The continuous monitoring of these critical components enables the early detection of potential failures, and timely intervention can help prevent catastrophic failures that could lead to accidents.

Research on UAV fault detection methods falls into three categories: knowledge-based, model-based, and data-driven methods [18–20]. Knowledge-based approaches depend on expert understanding of the system being diagnosed. These methods detect faults using rules and heuristic knowledge. Knowledge-based approaches are particularly useful when the system being diagnosed is well-known and failure modes are clearly identified. However, they require a significant amount of work to develop and maintain as well as they can be ineffective in diagnosing complex systems.

Model-based methods utilize analytical or simulation models to describe and estimate system behaviour [21–23]. Anomalies are detected by comparing measured and estimated signals that represent the discrepancy between the actual and estimated behaviour of the system. Cao et al. [24] discussed fault detection methods for fixed-wing

E-mail address: erkancaner.ozkat@erdogan.edu.tr.

https://doi.org/10.1016/j.jestch.2024.101702
Received 14 November 2023; Received in revised form 15 April 2024; Accepted 5 May 2024
Available online 13 May 2024

UAVs using extended attitude observer and range observer approaches. The extended status observer was designed for fault detection, while the interval observer handled both disturbances and faults. Similarly, Hamadi et al. [25] investigated a fault-tolerant method for quadrotor UAVs that experience both hardware and software sensor failures. To detect faults, the authors used both basic and extended Kalman filtering using signals derived from the GPS, IMU, and magnetometer. Although model-based approaches are robust and capable of detecting unknown faults, they face difficulties in developing accurate models and can incur computational costs. Both model-based and knowledge-based techniques rely on predefined parameters, which limits their applicability to UAVs operating in various flight situations. Improving adaptability is critical for effective fault diagnosis in dynamic UAV scenarios.

With the advancement of computational power, data-driven methods based on machine learning [26,27] and signal processing [28,29] have become a prominent topic of study in the field of anomaly detection in UAVs. These methods can capture the underlying complexity and variability of the system that knowledge and model-based models may not be able to effectively represent. Machine learning-based approaches are generally divided into two categories: supervised and unsupervised learning.

Supervised machine learning-based approaches train models on both normal and abnormal data samples and anomaly detection is based on a classification problem that distinguishes between healthy and faulty cases. For instance, Saied et al. [30] used a fault-tolerant active control approach with a support vector machine (SVM) classifier to detect and diagnose problems in the motors and rotors of a multi-rotor UAV. Altinos et al. [31] developed audio signal analysis methods to identify damage in motors, achieving good accuracy with fine decision tree (DT), SVM, and k-means nearest neighbour (kNN) classifiers. It is important to note that supervised learning-based techniques have limitations in detecting faults that are not explicitly trained during the model training phase. As the trained model learns only from the patterns present in the training dataset, it may encounter challenges in recognizing new failure patterns that are not present in the training data.

In contrast, unsupervised machine learning techniques can automatically learn complex patterns from raw data, making them more adaptable and efficient in collecting complex relationships. Unsupervised machine learning-based anomaly detection is becoming more popular due to its ability to process large, high-dimensional data and automatically extract complex features [32–34]. For instance, Jeon et al. [35] focused on detecting structural anomalies in UAVs, including damaged propellers or motors, which are vital to mission-critical operations. The authors used a long short-term memory (LSTM) autoencoder model to extract complex features from regular flight data, enabling accurate detection of structural anomalies during UAV flight. Lu et al. [36] suggested a deep learning-based system for fault identification in motors, monitoring the acceleration of the increase in motor temperatures to anticipate faults. Qi et al. [37] proposed a novel approach for identifying sensor faults in rotor-equipped UAVs using an adaptive threshold neural network (NN). This approach is notable for its ability to detect anomalies in-flight data, including important parameters such as acceleration, location, and angular velocity.

The sensor data generated during the operation of the UAV are time series data that provide information about its operational status, which includes regular and abnormal states. Anomaly detection using time series forecasting involves predicting future time points based on historical data. Significant differences between predicted results and actual sensor data serve as indicators of possible anomalies that may occur in the UAV at the time of forecasting. This method is based on understanding historical patterns to predict normal behaviour and effectively detect abnormal deviations during real-time UAV operations. Although the aforementioned studies have achieved good results, they pay attention to constructing classification or regression models from raw signals but pay less attention to the frequency information of the degradation process. Another challenge is extracting features from multiple domains (i.e., time, frequency, and time–frequency domains) and then combining them into a single health indicator. This means it can be difficult to determine the most effective way to combine these features into a single health indicator that accurately represents the overall health of the UAV. In addition, the presented literature emphasizes that the dominant models developed are offline, meaning that the decision-making process cannot be carried out in real-time. This limitation poses a significant challenge to the widespread use and commercialization of offline methods, especially for amateur drone pilots who lack the technical resources and experience necessary to use this methodology effectively. Therefore, a method called Wavelet Scattering Long Short-Term Memory Autoencoder network was adopted to identify the blade propeller damage fault in UAVs based on the gathered vibration signals. The main contributions of this study are as follows:

i The study presents an end-to-end anomaly detection method that combines the advantages of wavelet scattering and LSTM autoencoder to capture both time and frequency domain information in the input vibration signal. The LSTM autoencoder can learn the temporal patterns in the input data, while the wavelet scattering can capture the dynamics and interactions of different frequency components of the signal.

ii There is no requirement to manually extract features from the vibration signal. This allows for the direct input of the original signal gathered during flight, including disturbances, into the proposed network. This is due to its ability to extract non-linear dependencies and different scales of variation in the signal that are invariant to small perturbations, which makes it particularly useful for applications where the signal is noisy or contains uncertainties.

iii The proposed network includes dropout layers during model training to prevent over-fitting, which can improve the performance and robustness of the network. The use of four LSTM layers, two at the encoder level and two at the decoder level integrates feature extraction, feature dimension reduction, and pattern recognition to achieve end-to-end fault identification.

iv The proposed network is based on identifying deviations from the learned patterns of normal behaviour using unsupervised machine learning with unlabelled data without needing prior knowledge of which instances are abnormal. Therefore, it can offer a more flexible solution to anomaly detection in real-time scenarios.

The remainder of the paper is structured as follows: Section 2 presents the proposed methodology for anomaly detection in UAVs based on the Wavelet Scattering Long Short-Term Memory Autoencoder. Section 3 discusses the experimental setup and gives the findings from both the experiments and the proposed network. Finally, Section 4 provides the conclusions of this study and the directions for future research.

2. Methodology

The goal of anomaly detection is to identify patterns in signals that indicate a fault or potential problem. To achieve this, the proposed wavelet scattering LSTM autoencoder network extracts a set of scattering coefficients from the input signal using wavelet scattering. The scattering coefficients are then fed to the LSTM autoencoder, which reconstructs the original signals. The proposed network was trained with a collection of normal data, yielding a model that can reconstruct such data accurately and with minimal deviation. However, when the developed model encounters an abnormal signal and attempts to reconstruct the signal, the difference between the reconstructed

signal and the actual signal increases dramatically. When the difference exceeds a certain threshold, the model will generate an alert and detect an anomaly. The following sections will present brief descriptions of wavelet scattering and LSTM autoencoder techniques, followed by an in-depth review of the training process for the proposed network.

2.1. Wavelet scattering

The wavelet scattering transform is a set of operations that analyse a signal or image using a cascade of wavelet transforms and modulus non-linearities, resulting in a set of coefficients that capture information about the signal or image at multiple scales and orientations. These coefficients create a representation that is both sparse and resistant to distortion [38]. Wavelet scattering is a powerful and effective fault diagnosis technique because it captures non-linear dependencies and multiple scales of variation in the signal.

Wavelet scattering is the combination of wavelet and scattering transforms. It is designed to extract information from signals that are resistant to minor changes and to capture non-linear relationships between frequency components. The input signal is first decomposed into its frequency components. The wavelet coefficients are then sent through a non-linear operator to capture the non-linear dependencies in the signal. Finally, a pooling procedure, such as summing or averaging, is applied to the wavelet coefficients to produce the scattering coefficients. The wavelet transform decomposes the signal into its frequency components, whereas the scattering transform preserves information about the non-linear relationships between these frequency components.

The formulation of wavelet scattering can be described as follows. Given a signal x(t), the wavelet transform is applied to obtain wavelet coefficients $W_\lambda x(t)$. The wavelet transform is defined as:

$$W_\lambda x(t) = x(t) \otimes \psi_\lambda(t) \tag{1}$$

where $\otimes$ represents the convolution operation, and $\psi_\lambda(t)$ is the wavelet basis function which is the scaled and translated version of a mother wavelet function ψ. The mother wavelet function ψ is a fixed, non-stationary waveform that serves as the basic building block for the wavelet basis functions. By varying the scale and translation parameters, the wavelet basis function can be adapted to represent signals at multiple scales and locations in a compact and stable manner. Next, the wavelet coefficients are fed into a non-linear operator U, which captures the non-linear dependencies between the coefficients and given as:

$$U_\lambda x(t) = |W_\lambda x(t)| = |x(t) \otimes \psi_\lambda(t)| \tag{2}$$

This nonlinear operation extracts the amplitude of wavelet coefficients while discarding phase information. The wavelet scattering transform is thus defined as the repeated application of these operations across different scales and orientations. This produces a set of coefficients that contain information about the signal or image at multiple scales and orientations. Let U_m be the scattering propagator, which aggregates all the magnitudes of the wavelet coefficients and is represented as:

$$U_m = \{U_{\lambda_1}, U_{\lambda_2}, \dots, U_{\lambda_m}\} \tag{3}$$

Finally, the magnitude of the wavelet coefficients is aggregated through a pooling operation such as summing or averaging to obtain the scattering coefficients $S_j x(t)$. The mathematical formulation of wavelet scattering is as follows:

$$S_j x(t) = |||x(t) \otimes \psi_{\lambda_1}(t)| \otimes \psi_{\lambda_2}(t)| \cdots \otimes \psi_{\lambda_m}| \otimes \phi_j \tag{4}$$

where ϕ_j is the scaling function that provides an averaging operation over time. In this approach, the wavelet scattering transform employs the wavelet coefficients, the non-linear operator, and the pooling operation to produce a compact, multi-scale representation of the original signal that captures both its local and global structures. The wavelet scattering coefficients $S_j x(t)$ describe the key features and structures in the data, making them a useful tool for signal and image analysis.

2.2. Long Short-Term Memory (LSTM) autoencoder

The LSTM autoencoder is a specific type of autoencoder architecture in which both the encoder and decoder are built using LSTM networks [39,40]. Autoencoders are unsupervised neural networks used for dimensionality reduction and feature learning, whereas LSTMs are recurrent neural networks used to analyse sequential data. The LSTM autoencoder can learn patterns in sequential data over long sequences, making it ideal for time series forecasting and anomaly detection applications. In an LSTM autoencoder, the encoder maps the input data to a reduced dimensional representation by encoding the sequence into an LSTM memory cell, and the decoder reconstructs the original data by decoding the compressed representation with a reverse LSTM layer. The architecture allows the LSTM autoencoder to recognize temporal patterns in input data and produce a compressed representation suitable for anomaly detection. Nonetheless, using LSTMs in an autoencoder structure might be resource-intensive, potentially leading to overfitting if not adequately managed due to the complexity of the network. Despite this, the LSTM autoencoder has the advantage of collecting both temporal and spatial data properties, making it an effective tool for forecasting time series and detecting anomalies.

Given a sequence of input $X = \{x_1, x_2, \dots, x_t\}$ the encoder maps the sequence to a lower dimensional latent representation $Z = \{z_1, z_2, \dots, z_t\}$ using the encoding function h_{enc} as follows:

$$Z = h_{enc}(X) \tag{5}$$

The decoder maps the latent representation back to the original data using the decoding function h_{dec} as follows:

$$Y = h_{dec}(Z) \tag{6}$$

where Y is the reconstructed sequence of the given X. In an LSTM autoencoder, both the encoder ($\mathrm{h}h_{enc}$) and decoder (h_{dec}) functions are LSTM networks. The LSTM network consists of a cell state C_t and three gates: i_t for input, f_t for forget, and o_t for output. The cell state C_t represents the long-term memory of the network, and gates regulate the flow of information into and out of the cell state. The input gate selects what information should be placed in the cell state, the forget gate determines which information should be extracted from the cell state, and the output gate determines which information should be output from the cell state. The LSTM network updates the cell state and the output at each time step t as follows:

$$f_t = \sigma\left(W_f\left(h_{t-1}, X_t\right) + b_f\right) \tag{7}$$

$$i_t = \sigma\left(W_i\left(h_{t-1}, X_t\right) + b_i\right) \tag{8}$$

$$\tilde{C}_t = tanh\left(W_c\left(h_{t-1}, X_t\right) + b_c\right) \tag{9}$$

$$C_t = f_t C_{t-1} + i_t \tilde{C}_t \tag{10}$$

$$o_t = \sigma\left(W_o\left(h_{t-1}, X_t\right) + b_o\right) \tag{11}$$

$$h_t = o_t tanh\left(C_t\right) \tag{12}$$

where h_{t-1} is the previous and h_t is the current output of LSTM, W_f, W_i, W_o are the weights matrix of forget, input, output cells, b_f, b_i, b_o are the biases parameters, C_{t-1} is the previous, $\tilde{C}_t$ is the candidate and C_t is the current activation functions, respectively. The LSTM Autoencoder is trained to minimize the reconstruction loss, which measures the difference between the original and the reconstructed sequence of input X.

2.3. Proposed network for anomaly detection

This work presents an end-to-end anomaly detection method that combines the advantages of wavelet scattering and LSTM autoencoder to capture both time and frequency domain information in vibration signals. Wavelet scattering is employed in the network to detect anomalies because of its ability to execute multi-resolution analysis. This enables direct input of raw flight data, removing the requirement for manual extraction of frequency domain features. The LSTM autoencoder, which involves a cell state and three gates (input gate, forget gate, and output gate), is good at detecting contextual anomalies since it can handle effectively sequential data.

To evaluate UAV vibration signals, a signal duration of 1 s was chosen to provide a comprehensive and detailed view of the vibrations and facilitate the detection of subtle patterns or anomalies. The wavelet scattering network was designed by using an invariance scale of 0.2 s to control the level of invariance of the output features. The network contained 4 wavelet filters per octave in the first layer, while only 1 filter was used in the next layer. This configuration yielded a feature matrix of 28 distinct pathways and 59 samples, where each path represents a unique set of scattering coefficients calculated for a given input signal. These calculated wavelet scattering coefficients were then used as input for an LSTM autoencoder aimed at anomaly detection.

The encoding phase of the network is comprised of interconnected layers, starting with an initial LSTM layer followed by a rectified linear unit (ReLU) activation function. Subsequently, a second LSTM layer is integrated, followed by a dropout layer utilized for regularization, and finally capped with another ReLU activation function. The first LSTM layer is structured with a cell count equivalent to the number of scattering coefficients generated by the Wavelet Scattering method, specifically 30 cells. To address the vanishing gradient issue, the second LSTM layer is configured with half the number of scattering coefficients, namely 15 cells. Within the network architecture, ReLU serves as the activation function, facilitating nonlinear transformations to tackle the vanishing gradient challenge. Additionally, a dropout layer is employed as a regularization technique, randomly discarding 20% of the input during training to mitigate overfitting. This strategic combination not only enhances the robustness of the network but also ensures effective training by minimizing the risk of overfitting the training dataset.

In the decoding process, improvements have been made to improve the reconstruction of the input sequence. This involves adding a specific layer that mimics the output of the last LSTM layer in the encoding stage. The decoding architecture begins with an initial LSTM layer, followed by a dropout layer, a ReLU activation function layer, a secondary LSTM layer, and finally a ReLU activation function layer. Notably, the number of LSTM cells in the decoder is arranged in the opposite order compared to the encoder, with 15 cells in the first LSTM layer and 30 cells in the second LSTM layer. Finally, the output from the last decoder layer is fed into a regression layer, which produces the reconstructed signal.

The training process will involve fine-tuning the weights and biases of the network employing the Adam optimization method until a maximum of 500 epochs are reached. To reduce overfitting, a random sampling process will be applied after each epoch. Throughout training, the performance of the model will be evaluated using the validation set, and the model with the lowest validation loss will be selected as the best model. The architecture of the proposed Wavelet Scattering LSTM Autoencoder network is depicted in Fig. 1.

The methodology for implementing the proposed network comprised several sequential steps. The first step involved preprocessing the acquired signal using outlier detection to ensure that the signal behaviour was accurately represented. This involved the identification and removal of data points that deviate more than three standard deviations from the mean in the vibration signal. Subsequently, the signal was segmented to create a format suitable for the proposed wavelet scattering LSTM autoencoder network. In the third step, the network underwent training using a designated set of training data, aiming to generate a model capable of accurately reconstructing the training data with minimal deviation. However, when a faulty signal was reconstructed by the trained network, a notable increase in disparity between the reconstructed signal and the original faulty signal was observed. The final step involved defining an anomaly score and establishing a threshold based on statistical distribution to distinguish between normal and abnormal data.

Fig. 2 illustrates the general methodology for evaluating UAV vibration signals using wavelet scattering and an LSTM autoencoder network. Notably, in this study, the first two throttle positions were considered normal operating conditions due to their association with stable flight conditions, despite the utilization of groove propeller blades at low speeds.

The selection of an appropriate threshold for anomaly detection is not well-defined and varies by application. The interpretation of the anomaly score and the threshold for triggering a warning signal can be likened to the statistical process control (SPC) problem. In both contexts, the objective is to establish a threshold that effectively distinguishes normal operating conditions from potential anomalies. In this study, the mean-absolute error (MAE) was utilized to define the anomaly score, and the anomaly score threshold was chosen as 1.5 times the interquartile range (IQR) of the data, which measures the spread of the middle 50% of the data and is robust against outliers. In contrast, the conventional 6-sigma approach for SPC sets control limits at three times the standard deviation from the mean, making it sensitive to outliers. While IQR is versatile and not reliant on a normal distribution assumption, the 6-sigma approach is commonly used in control charts for detecting significant deviations from the mean, assuming a normal distribution for accurate interpretation. The pseudo-code of the network is shown in Algorithm 1.

Algorithm 1 The Pseudocode of the Wavelet Scattering LSTM Autoencoder

Require: Load time-series signal X (Vibration signals)
Require: Define constants: Sampling Frequency fs, Window Size w_s
Require: Define Wavelet Scattering architecture
Require: Define LSTM Autoencoder architecture
for $replicaiton = 1$ to 3 **do**
  for $axes = 1$ to 3 **do** ▷ Vibration signals from x, y, and z axes
    Segment signal X into 1-second intervals
    Apply wavelet scattering transform on signal segment
    Extract features $SAll$ from the wavelet scattering
    Split $SAll$ into training, validation, and verification sets
    Initialize LSTM autoencoder model
    Train LSTM autoencoder on the training set
    Compile the model with appropriate loss function and optimizer
    Evaluate model on the validation set
    Reconstruct each 1-second segment
Require: Mean Absolute Error (MAE) between the original and reconstructed segments for fault detection
    Compute MAE on training, validation, and verification sets
    Calculate threshold MAE based on the validation set
    if Computed MAE $\geq$ threshold MAE **then**
      Generate a warning signal for anomaly detection
    end if
    Plot original signal, throttle, and MAE over time
    Save plots
  end for
end for

3. Results & discussions

3.1. Experimental setup

The focus of this research study was a DJI M600 multirotor UAV that had 6 rotors, each fitted with 2 blades. In addition, the UAV was connected to the ground platform using cables to prevent it from flying over the laboratory as it was not physically practical. This

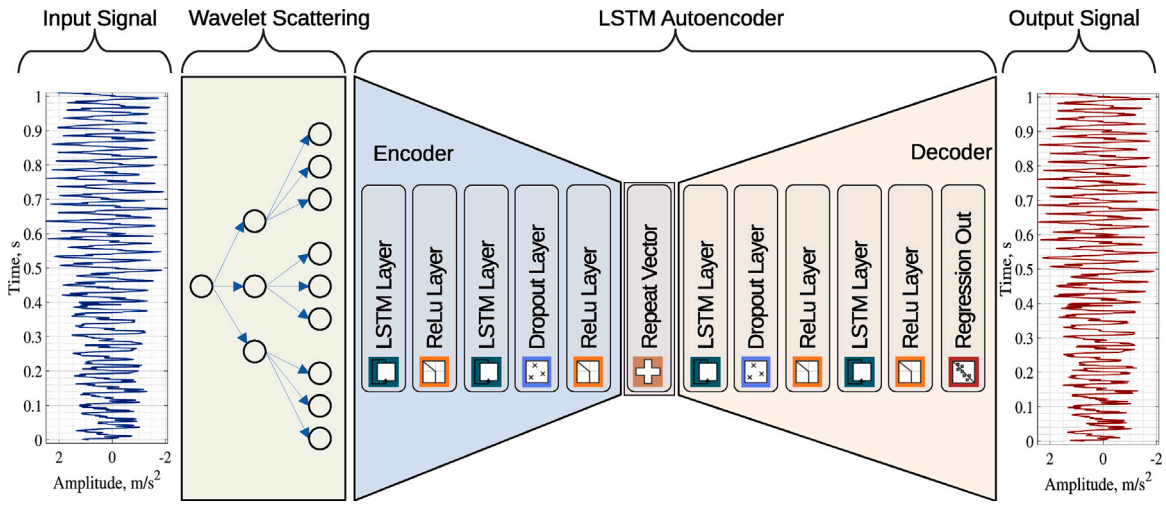

Fig. 1. The architecture of the proposed Wavelet Scattering LSTM autoencoder network.

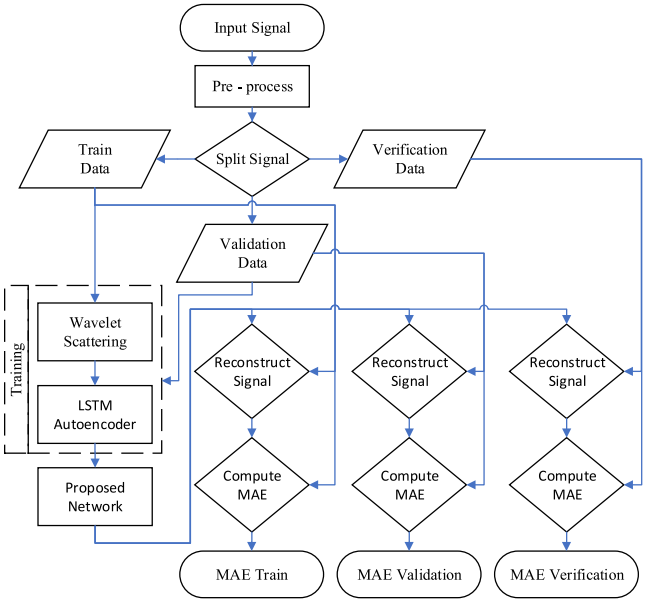

Fig. 2. Overview of the methodology flow for analysing UAV vibration signals using wavelet scattering and LSTM autoencoder network.

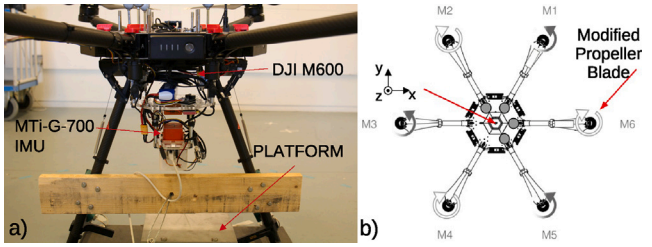

Fig. 3. The experimental setup: (a) DJI M600 UAV, platform and MTi-G-700 IMU, (b) Top-down view of the UAV. The propeller subject to modifications will be mounted at rotor M6.

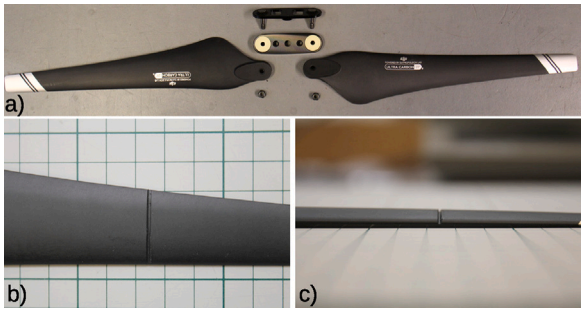

Fig. 4. The 2170R Folding Propeller: (a) Disassembled, modified with a groove (b) Top view, (c) Front view.

precaution was taken to prevent potential damage to the UAV during the experiments. Despite being tethered, the UAV remained airborne, allowing for meaningful data collection in a controlled environment.

The Inertial Measurement Unit (IMU) Xsens MTi-G-700 IMU was vertically aligned with the centre of gravity of the UAV, and it was placed immediately underneath the centre console. It was linked to the onboard computer via USB, where the signals were read and recorded at a frequency of 800 Hz. The Xsens MTi-G-700 IMU provides 3D linear acceleration, 3D angular velocity, and 3D magnetic field measurement. During the experiments, the Xsens MTi-G-700 IMU records only raw data, despite having filtering options. This choice preserves the original, unprocessed measurements, offering flexibility for later analysis and the application of specific filtering techniques as required.

The Xsens MTi-G-700 IMU features an orientational precision of 0.25 degrees in roll, 1 degree in pitch and yaw, a horizontal position accuracy of 1 m, a vertical position accuracy of 2 m, and a velocity accuracy of 0.1 m/s. The IMU has a full-scale range of 78 m/s^2 for the accelerometer and 625 °/s for the gyroscope. Fig. 3 presents an overview of the experimental setup, including the DJI M600 multirotor UAV, platform, and MTi-G-700 IMU. The 2170R Folding Propellers, which consist of a central hub and two blades were utilized in the experiments.

To induce vibration, one of the blades was particularly modified to form a groove around 75% of the blade thickness, placed 9 cm from the tip of the blade, using a CNC machine with a 1.5 mm cutting tool. Fig. 4 depicts a disassembled propeller and a propeller blade modified with a groove. During the experiments, the accelerometer signals were gathered systematically by observing the UAV at each of the 10 predetermined throttle positions, beginning with its initial healthy state and advancing to failure. A 40-s interval was maintained at each throttle position to capture comprehensive data across different operational states. To enhance the reliability of the results, the entire experiment was meticulously replicated three times.

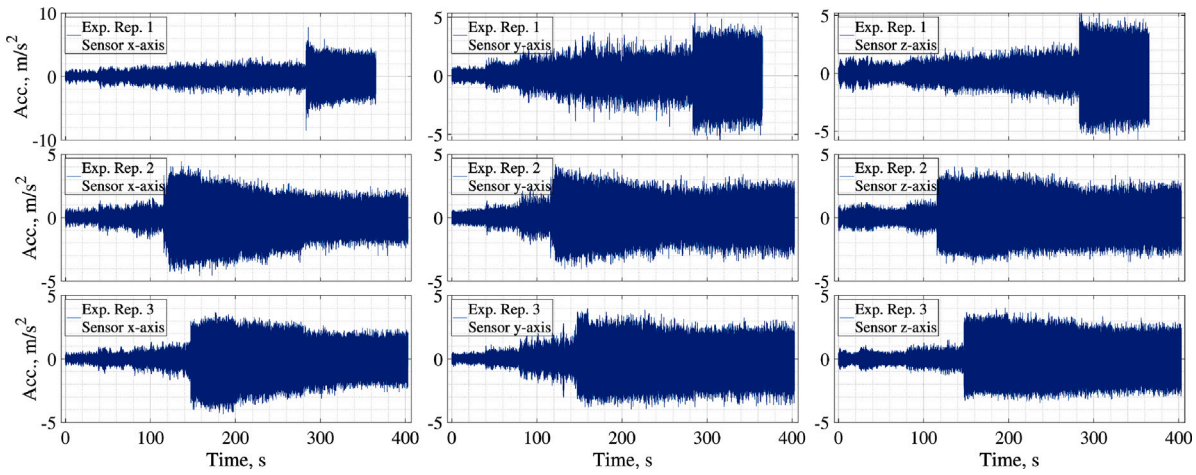

Fig. 5. Time-domain vibration signals recorded from all axes for each experimental replication.

3.2. Experimental results

The commercial UAVs are produced with high-quality standards to ensure their safety and reliability during flights. The intentional modification of one propeller blade in this study aims to simulate real-world challenges faced by UAVs during autonomous tasks, such as collisions with unexpected objects or exposure to strong winds that can push UAVs into solid obstacles. Blade defects, including fractures or distortions, arising from such incidents can compromise the stability and manoeuvrability of the UAV during flight. When a UAV collides with an object, it immediately undertakes actions to regain stability, inducing uneven rotor speeds, with some rotating at a faster pace than others, thereby producing vibrations. Furthermore, the damaged blade emits a sound that is distinct from the regular noise associated with the UAV in its normal operational state.

Fig. 5 illustrates the captured vibration signals, providing a graphical representation of the acceleration values along the x, y, and z-axes for all experimental replications. It is worth mentioning that the propeller blade broke at throttle positions of 80%, 30%, and 40% in the first, second, and third replications, respectively. Upon observation, it can be noted that the trend across each replication is consistent and characterized by a sharp increase in the magnitude of the vibration signal at the time of failure. The analysis of the vibration signal in the time domain reveals an absence of significant fluctuations before the occurrence of failure, whereas a sudden change occurs at the time of failure. This observation highlights the need to look at alternative domains to study the vibration signal to provide a more comprehensive understanding of the underlying mechanisms leading to failure.

Fig. 6a presents a graphical representation of the spectral (i.e., frequency-domain) and spectrogram (i.e., time–frequency-domain) analysis of the raw vibration signal acquired from the x-axis of the third replication. These visualizations serve as a tool to analyse and understand the frequency content and temporal dynamics of the signal. Prior to analysing the vibration signal responses in both the frequency and time–frequency domains, a statistical characterization of the vibration signal was performed. Specifically, the mean and standard deviation of the vibration signal at each throttle position were calculated. Subsequently, any data points that deviated more than three standard deviations from the mean were identified and removed from the vibration signal to ensure a more accurate representation of the signal behaviour. The mean, standard deviation, outliers, and throttle positions are shown in Fig. 6b.

The spectrum of the signal depicted in Fig. 6c serves as a visual representation of its frequency composition and is useful in determining the dominant frequency components. The spectrum analysis reveals that the peak frequency is approximately 60 Hz, and the dominant frequencies are concentrated within a narrow range between 50 Hz and 70 Hz. It is important to note that the presence of multiple peaks in the frequency spectrum can be attributed to the presence of unbalanced masses, which induce vibration due to their rotation or the harmonics of the fundamental rotational frequency. In the frequency spectrum, peaks can be detected at 150 Hz, 200 Hz, and 300 Hz. On the other hand, the spectrogram depicted in Fig. 6d offers a visual representation of how the frequency content of the signal evolves over time, which is valuable for detecting temporal variations in the signal and characterizing dynamic changes in its frequency content. As the throttle position is increased, there is a slight shift in the dominant frequencies associated with the throttle position from 45 Hz to 50 Hz, which persists until 80 s. From this time until failure, the dominant frequencies are observed to be around 100 Hz, and after failure, they remain nearly constant at approximately 60 Hz. This phenomenon could be an indication that the propeller blade was flapping before breaking. Furthermore, significant dominant frequencies at 150 Hz, 200 Hz, and 300 Hz can also be identified, which exhibit a slight increase over time, as depicted in the accompanying spectrum graph.

Fig. 7 illustrates vibration signal analysis from all axes across all replications, offering a comprehensive understanding of the temporal and frequency characteristics. The experimental setup involved intentionally modifying one of the UAV blades with a groove comprising about 75% of the blade thickness. This intentional modification did not cause the blade to break before the experiments were conducted. Instead, during the experiments, the blade was broken at the location of the groove, thereby inducing a structural fault. The analysis of temporal patterns across different axes revealed a consistent pattern between the y and x axes for all replications. While spectrogram graphs obtained from different axes within the same replication exhibited similar frequency patterns, it was observed that the frequency patterns in different replications within the same axis corresponded to the timing of the fault. Notably, the z-axis had lower frequency amplitudes than the x and y axes, with the main frequency shifting slightly from 45 Hz to 50 Hz just before failure. Following the failure, the existence of many dominating frequencies shows a complicated vibration pattern incorporating fundamental blade rotation, higher harmonic components, or resonances. This intricate pattern suggests that the structural fault in the blade led to dynamic changes in the vibration characteristics, manifesting as a combination of fundamental and higher-order frequency components. Furthermore, notable frequencies at 150 Hz, 200 Hz, and 300 Hz exhibited a gradual increase over time, potentially linked to harmonic components within the system.

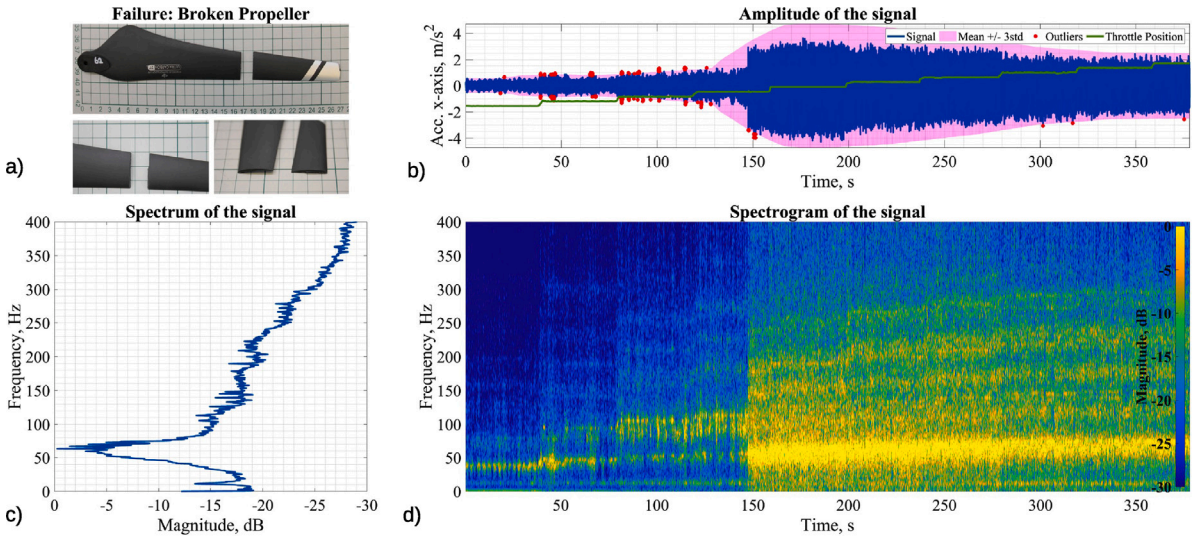

Fig. 6. Vibration data analysis from the *x*-axis during the 2nd replication: (a) Visual representation of a broken propeller, and signal analysis in (b) time-domain, (c) frequency-domain, and (d) time–frequency-domain.

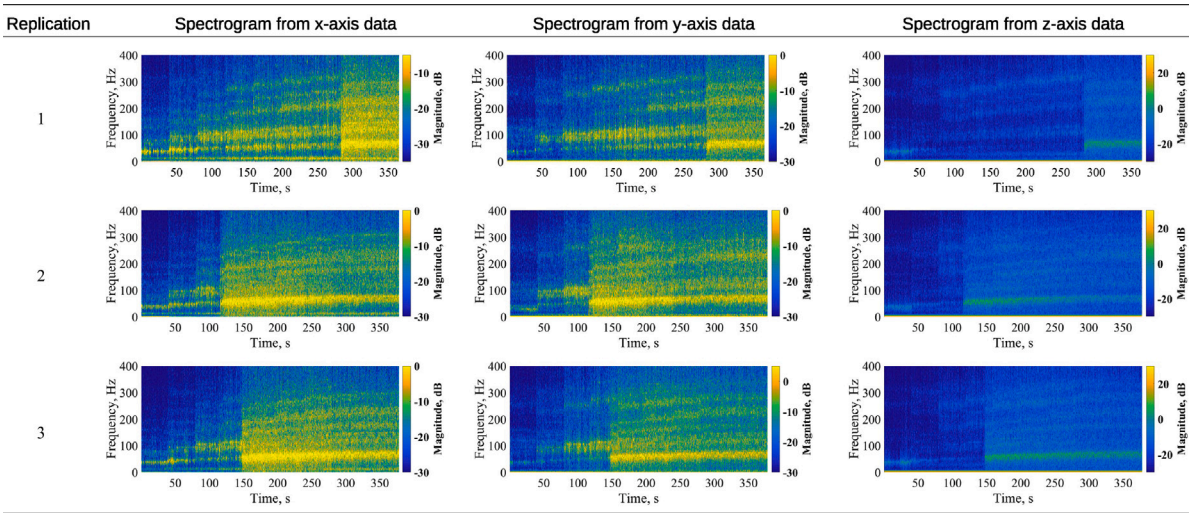

Fig. 7. Spectrogram results of vibration signal analysis gathered from all axes across all replications.

3.3. Anomaly detection performance

In this study, the proposed wavelet scattering LSTM autoencoder network was evaluated for its performance in analysing vibration signals captured along all three axes. Figs. 8–10 display the vibration signals and corresponding anomaly detection results for all three axes of the first, second, and third experimental replications. It is noteworthy to mention that prior to the experiments, the propeller blade was found to be fully intact with no apparent structural defects. However, at the end of each experiment, it was observed that the propeller blade was consistently broken. As a result, training and validation datasets were selected from the earliest recordings to increase the likelihood that these datasets contain only recordings without the presence of the fault. The training dataset was formed using the first two throttle positions (up to 80 s), while the next throttle position (up to 120 s) was used to create the validation set. The remaining throttle positions were held out as the verification dataset.

The proposed network is designed to produce a reconstructed vibration signal output of 1-s length, in response to a 1-s vibration signal input. In the case where the computed MAE value between the reconstructed and the original signal surpasses a pre-defined threshold, a warning is triggered to indicate the presence of an anomaly in the vibration signal. In light of this, it can be observed that Figs. 8–10 indicate that warning signals were generated from each axis in all repetitions prior to the failure. Furthermore, it could be deduced that the earliest warnings were detected in the *y*-axis signals, while the latest warnings were detected in the *z*-axis. This observation may be attributed to the mass imbalance in the propellers, which may lead to oscillations in the XY plane. Since the XY plane is the plane in which the rotors rotate, it is more sensitive to variations in thrust produced by the rotors, making it more vulnerable to damage. The presence of damaged propellers may introduce changes in the UAV dynamics, resulting in higher magnitudes of vibration, which can be detected in the *y*-axis signals. Conversely, as the *z*-axis is less affected by the imbalance of the propellers, the damage is less likely to manifest in this direction, resulting in the later detection of warnings.

The results of this study indicated that the proposed network could provide an early warning for potential faults in the system. In the first replication, the first warnings based on the *x* and *y*-axis data were received within 100 s, while the first warning based on the *z*-axis data was received after 130 s. Notably, the MAE values calculated for the *y*-axis data in the verification section were highly fluctuating, suggesting

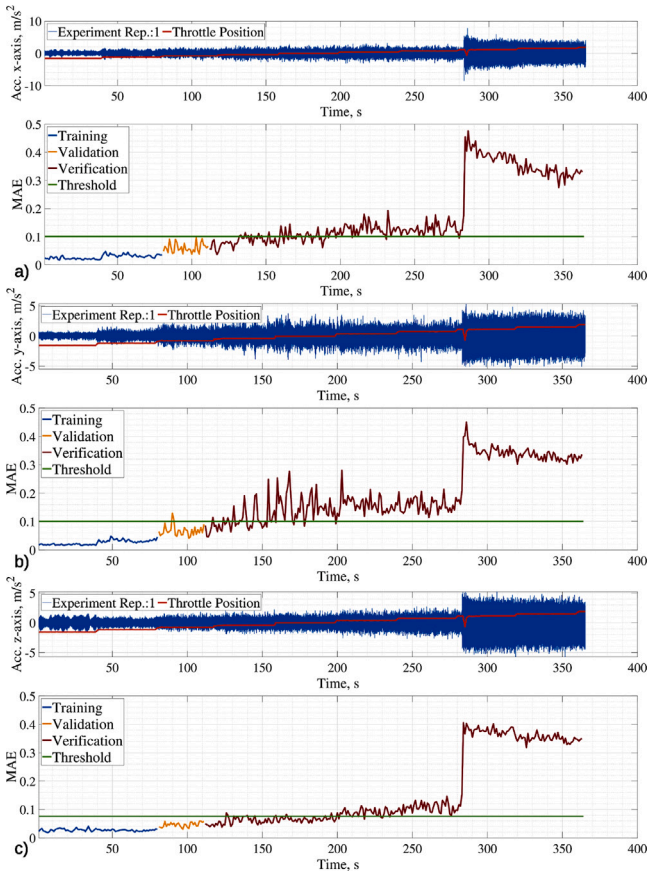

Fig. 8. Vibration data and anomaly detection results for the (a) *x*-axis, (b) *y*-axis, and (c) *z*-axis of the 1st experimental replication.

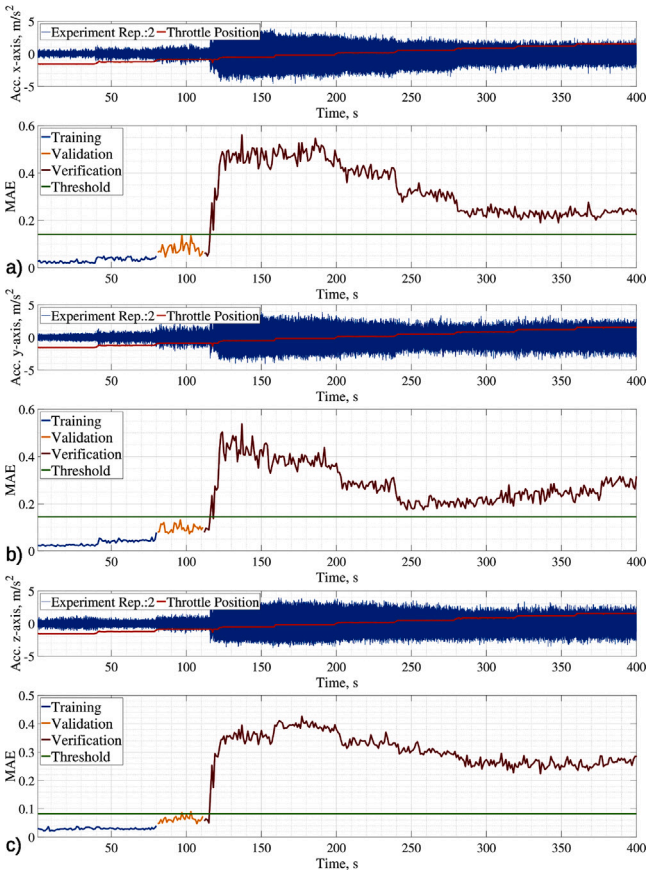

Fig. 9. Vibration data and anomaly detection results for the (a) *x*-axis, (b) *y*-axis, and (c) *z*-axis of the 2nd experimental replication.

an impending failure. The failure was recorded at 283 s during the first replication, approximately 180 s after the first warning was received. In the second replication, the MAE values derived using data from all three axes followed a similar trend. The first warning was triggered at 90 s, and the failure occurred approximately 30 s later. In the third replication, the MAE values calculated for the *y*-axis data fluctuated significantly more than the MAE values calculated for the other axes. The first warnings were received within 100 s based on the *x* and *y*-axis data, while 130 s based on the *z*-axis data. The failure was recorded at 147 s.

3.4. The performance evaluation of the proposed network

This section assesses the performance of the proposed network under different configurations. It is crucial to note that the proposed network in this study does not forecast the precise timing of faults but rather assesses whether the vibration signal contains anomalies. Therefore, the assessment of the proposed network relies on classification metrics such as accuracy, sensitivity, and error rate. Specifically, identifying a warning signal before a failure is denoted as a False Negative, and recognizing a warning signal after a failure is termed a True Negative. Conversely, failure to identify a warning signal pre-failure is considered a True Positive, and the absence of a warning signal post-failure is labelled as a False Positive.

The architecture of the proposed network featured two LSTM layers in the encoder stage, with the first layer comprising 30 LSTM cells and the second layer comprising 15 cells. A dropout layer, serving as a regularization technique, was inserted between the LSTM layers to prevent overfitting by randomly discarding 20% of the input. The decoder was also structured with two layers, where the first layer housed 15 cells, the second layer housed 30 cells, and a similar dropout layer was employed. The ablation study was executed in two phases, involving the removal of dropout layers in the first stage and the removal of second LSTM layers in the second stage. Table 1 compares the effectiveness of the network with different settings. In the context of anomaly detection for UAVs based on vibration signals, accuracy is a measure of how well the proposed network can correctly identify and classify instances as either normal (pre-failure) or anomalous (post-failure). Specificity represents the rate of correctly identified normal data, and the error rate values indicate the fraction of misclassifications for each replication and network configuration. The full network exhibits robustness, achieving high accuracy and sensitivity with low error rates across replications for all axes. Upon the removal of dropout layers, a marginal reduction in accuracy and sensitivity is observed, for instance, dropping to 0.763 and 0.642 in the 1st replication. Further removal of both dropout and the second LSTM layers amplifies this effect, resulting in accuracy values of 0.766, 0.639, and 0.939 for the 1st, 2nd, and 3rd replications, respectively. Notably, the second replication consistently demonstrates superior performance across configurations regardless of the configuration. A lower error rate suggests better overall performance in terms of minimizing misclassifications in the UAV vibration signal data. The error rates, however, show slight increases, emphasizing the trade-offs associated with model simplification. In reality, as an anomaly is likely to lead to the overall failure of the UAV, achieving high sensitivity is more important than the error rate. Considering results across all replications and axes, the best-performing configurations, ranked from best to worst, are the full model, dropout layers removed from the model, and dropout and 2nd LSTM layers removed from the model.

Table 1
The ablation study results show the performance of the proposed network.

Network type	Replication	Accuracy			Sensitivity			Error Rate		
		x-axis	y-axis	z-axis	x-axis	y-axis	z-axis	x-axis	y-axis	z-axis
Proposed Network	1st	0.780	0.725	0.716	0.714	0.643	0.643	0.220	0.275	0.284
	2nd	0.997	1.000	0.995	0.991	1.000	1.000	0.003	0.000	0.005
	3rd	0.957	0.989	0.989	0.890	0.973	0.973	0.043	0.011	0.011
Dropout layers removed	1st	0.763	0.642	0.694	0.693	0.536	0.536	0.237	0.358	0.306
	2nd	0.997	1.000	0.995	0.991	1.000	1.000	0.003	0.000	0.005
	3rd	0.976	0.984	0.981	0.938	0.959	0.959	0.024	0.016	0.019
Dropout & 2nd LSTM layers removed	1st	0.766	0.639	0.744	0.696	0.532	0.532	0.234	0.361	0.256
	2nd	0.997	0.997	0.995	0.991	0.991	0.991	0.003	0.003	0.005
	3rd	0.939	0.910	0.981	0.898	0.767	0.767	0.061	0.090	0.019

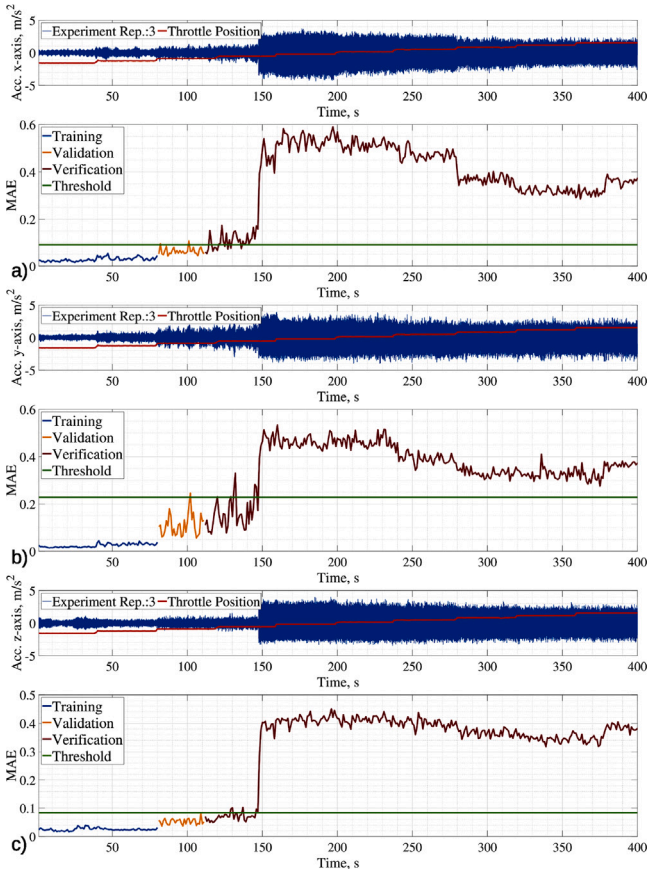

Fig. 10. Vibration data and anomaly detection results for the (a) *x*-axis, (b) *y*-axis, and (c) *z*-axis of the 3rd experimental replication.

3.5. Discussions & limitations

UAVs are becoming more common in various industries and applications, raising several safety issues, including how to handle malfunctions and subsequent crashes. One solution is to monitor the health of UAVs and predict or detect system faults in advance, allowing the operator or system to perform an emergency or crash landing. In the scope of this study, a data-driven approach was employed for anomaly detection, which demonstrated its efficacy in successfully identifying anomalies within the vibration signals before the occurrence of propeller blade damage.

It is vital to highlight that the investigation was carried out in a controlled laboratory environment using a single UAV model. Despite this constraint, the network is scalable to real-world scenarios because its architecture is designed to dynamically learn key features from input data, not limited to the vibration signals. This feature learning capacity is critical since it enables the network to adapt to a variety of UAV types and operating circumstances. Furthermore, the proposed approach is based on evaluating vibration signals that are directly related to structural degradation. However, the proposed network has the potential to detect a wide range of anomalies, including electrical or software faults, as long as the input signal can be analysed as a time series. Monitoring the temporal evolution of input data allows for the detection of deviations from normal behaviour, which can indicate impending anomalies and eventually failures in UAVs. However, gathering a substantial amount of labelled data can be difficult and frequently necessitates specialist knowledge, especially when dealing with unusual or unexplained anomalies.

The results highlight the effectiveness of the proposed network in consistently providing early warnings across all axes, with the *y*-axis exhibiting the earliest signals and the *z*-axis the latest. This trend is attributed to propeller mass imbalances impacting the XY plane. The temporal lead time for warnings varied, occurring within 100 s, 90 s, and 100 s before failure events in the 1st, 2nd, and 3rd replications, respectively. The modification of the blade produced a complex vibration pattern containing fundamental rotation frequency, and higher harmonic components. Identifying specific frequencies such as 150 Hz, 200 Hz, and 300 Hz provides more detailed information about fault-induced dynamics. The combination of wavelet scattering for frequency analysis and the LSTM autoencoder for temporal monitoring is a novel approach that provides a complete understanding without the requirement for human feature extraction. However, this study has certain limitations, particularly in defining control limits for anomaly detection due to the unknown distribution of the data.

In this study, the IQR was employed to establish control limits, with the anomaly score threshold set at 1.5 times the IQR. Modifying the threshold value not only influences the warning signal received before a fault (false positive) but also impacts the warning signal received after a fault (false negative). The adjustment of this threshold plays a crucial role in determining the trade-off between detecting anomalies early and minimizing the occurrence of false positives or negatives, thereby influencing the overall performance and reliability of the anomaly detection system.

The practical implementation of the proposed scheme may face challenges when dealing with off-the-shelf UAVs, known for their limited customization options. Utilizing software development kits or collaboration with manufacturers could facilitate the deployment of the proposed network for anomaly detection.

4. Conclusions & future works

This research presents a wavelet scattering LSTM autoencoder network for anomaly detection. The key contributions of this work lie in the integration of two advanced techniques for anomaly detection: the novel use of wavelet scattering to analyse the frequency components of the vibration signal, providing a comprehensive understanding without manual feature extraction, and the implementation of an LSTM autoencoder to monitor the temporal evolution of frequency components, thus enabling anomaly detection over time. Moreover, the study underscores the significance of unsupervised machine learning methods

for anomaly detection since they allow for the identification of irregular patterns and outliers in data without the need for labelled data, thus enabling the detection of unforeseen anomalies in complex systems. The conclusions of this study can be given as follows:

i A deliberate modification was made to one of the propeller blades by cutting a groove 9 cm from the tip of the blade and covering approximately 75% of its thickness. This intentional modification did not cause the blade to break before the experiments were conducted. Instead, during the experiments, the blade was broken at the location of the groove, thereby inducing a structural fault. The propeller blade broke at approximately 280, 120, and 150 s for the 1st, 2nd, and 3rd replications. The spectrogram graphs showed that the main frequency shifted slightly from 45 Hz to 50 Hz in each replication. However, after failure, frequencies at 150 Hz, 200 Hz, and 300 Hz exhibited a gradual increase over time, suggesting the presence of harmonic components within the system.

ii The network proposed in the study was tested on collected vibration signals. Across all axes, the network consistently detected anomalies, with the *y*-axis showing the earliest warning and the *z*-axis the latest. This trend was attributed to propeller mass imbalances affecting the XY plane. The proposed network underwent training using exclusively normal data so that once trained it could successfully reconstruct normal data while failing on abnormal data. The MAE metric was employed to compute the reconstruction error, with anomalies detected when the MAE exceeded a predetermined threshold value, set at 1.5 times the IQR. According to the results, the lead time for warnings varied among the replications, occurring approximately 100 s, 90 s, and 100 s before failure events in the 1st, 2nd, and 3rd replications, respectively.

iii Considering the average flying altitudes typically around 100 m, and landing speeds ranging from 3 to 5 m/s of UAVs, this 30-s window provides a vital opportunity to detect anomalies and initiate corrective actions swiftly. With a safe landing altitude of only 1 to 3 m above the ground, this buffer is critical for performing corrective actions such as automatic landing or repositioning the UAV to avoid a collision.

To address the acknowledged limitations and enhance the effectiveness of the proposed methodology, future research efforts will focus as follows. First, alternative approaches will be investigated to determine control limits in anomaly detection within the context of time series analysis. In the current study, the IQR was employed to establish control limits and the anomaly score threshold was set to 1.5 times the IQR. One potential alternative for setting control limits and thresholds is the application of control charts from the statistical process control such as Shewhart charts. These charts are specifically tailored to detect deviations from expected behaviour by defining control limits based on statistical measures. Second, it is essential to consider external factors such as wind or specific mission parameters during UAV flights, which may introduce noise into the recorded data. This noise can potentially mask actual anomalies or might give false alarms. To address this, this future work will explore the applicability of a movement-based reconstruction error by incorporating additional sensor data, such as the gyroscope data already available in IMU. It will initially involve computing a movement score based on aggregating gyroscope and acceleration data from each axis at the given time. The movement score will then be integrated into the reconstruction error. A comparison will be made between the reconstruction error derived from the movement score and the normal reconstruction error. If the movement-based reconstruction error is significantly higher, the warning signal is attributed to the movement; otherwise, the warning is considered error-related. This approach aims to reduce incorrect predictions caused by movement. Third, the proposed network has the potential to detect not only structural damages but also other anomalies such as electrical or software faults. By analysing data from multiple sensors, including those that monitor electrical systems and software performance, the network can identify patterns or deviations that could indicate problems in these areas. This comprehensive approach helps ensure the overall safety and reliability of the UAVs by improving the feasibility and ability of the proposed network to provide early warnings of various types of anomalies. Furthermore, acquiring labelled data for rare anomalies remains a significant challenge, suggesting the need for innovative approaches and cooperative projects to improve anomaly identification in UAVs.

CRediT authorship contribution statement

Erkan Caner Ozkat: Conceptualization, Formal analysis, Methodology, Software, Visualization, Writing – original draft, Writing – review & editing.

Declaration of competing interest

The authors declare that they have no known competing financial interests or personal relationships that could have appeared to influence the work reported in this paper.

Acknowledgements

This work was partially supported in part by the Scientific and Technological Research Council of Turkey (TUBITAK) under the BIDEB-2219 Post-Doctoral Research Scholarship Program. The author would like to extend their sincere gratitude to Prof. Anders la Cour-Harbo for generously sharing their research data and providing access to the Drone Research Laboratory during the author's post-doctoral studies at Aalborg University, Denmark.

References

[1] C.A. Thiels, J.M. Aho, S.P. Zietlow, D.H. Jenkins, Use of unmanned aerial vehicles for medical product transport, Air Med. J. 34 (2) (2015) 104–108.
[2] S. Bijjahalli, R. Sabatini, A. Gardi, Advances in intelligent and autonomous navigation systems for small UAS, Prog. Aerosp. Sci. 115 (2020) 100617.
[3] E. Balestrieri, P. Daponte, L. De Vito, F. Picariello, I. Tudosa, Sensors and measurements for UAV safety: An overview, Sensors 21 (24) (2021) 8253.
[4] E.C. Ozkat, O. Bektas, M.J. Nielsen, A. la Cour-Harbo, A data-driven predictive maintenance model to estimate RUL in a multi-rotor UAS, Int. J. Micro Air Veh. 15 (2023) 17568293221150171.
[5] W.-H. Lai, S.-T. Tsai, D.-L. Cheng, Y.-R. Liang, Application of wavelet scattering and machine learning on structural health diagnosis for quadcopter, Appl. Sci. 11 (21) (2021) 10297.
[6] E. Walker, S. Rayman, R.E. White, Comparison of a particle filter and other state estimation methods for prognostics of lithium-ion batteries, J. Power Sources 287 (2015) 1–12.
[7] L. Xing, B.W. Johnson, Reliability theory and practice for unmanned aerial vehicles, IEEE Internet Things J. (2022).
[8] R. Puchalski, W. Giernacki, UAV fault detection methods, state-of-the-art, Drones 6 (11) (2022) 330.
[9] P. Yang, H. Geng, C. Wen, P. Liu, An intelligent quadrotor fault diagnosis method based on novel deep residual shrinkage network, Drones 5 (4) (2021) 133.
[10] O. Bektash, J.J. Naundrup, A. la Cour-Harbo, Analyzing visual imagery for emergency drone landing on unknown environments, Int. J. Micro Air Veh. 14 (2022) 17568293221106492.
[11] P. Yang, C. Wen, H. Geng, P. Liu, Intelligent fault diagnosis method for blade damage of quad-rotor UAV based on stacked pruning sparse denoising autoencoder and convolutional neural network, Machines 9 (12) (2021) 360.
[12] H. Shakhatreh, A.H. Sawalmeh, A. Al-Fuqaha, Z. Dou, E. Almaita, I. Khalil, N.S. Othman, A. Khreishah, M. Guizani, Unmanned aerial vehicles (UAVs): A survey on civil applications and key research challenges, Ieee Access 7 (2019) 48572–48634.
[13] M.H. Che Man, H. Haoliang, K.H. Low, Crash area estimation for ground risk of small unmanned aerial vehicles due to propulsion system failures, in: AIAA SCITECH 2022 Forum, 2022, p. 1506.
[14] S.A.H. Mohsan, N.Q.H. Othman, Y. Li, M.H. Alsharif, M.A. Khan, Unmanned aerial vehicles (UAVs): Practical aspects, applications, open challenges, security issues, and future trends, Intell. Serv. Robot. 16 (1) (2023) 109–137.

[15] J.-P. Yaacoub, H. Noura, O. Salman, A. Chehab, Security analysis of drones systems: Attacks, limitations, and recommendations, Internet Things 11 (2020) 100218.
[16] E.C. Ozkat, P. Franciosa, D. Ceglarek, Laser dimpling process parameters selection and optimization using surrogate-driven process capability space, Opt. Laser Technol. 93 (2017) 149–164.
[17] J. Cabahug, H. Eslamiat, Failure detection in quadcopter UAVs using K-means clustering, Sensors 22 (16) (2022) 6037.
[18] M. Zare, F. Pazooki, S.E. Haghighi, Hybrid controller of Lyapunov-based and nonlinear fuzzy-sliding mode for a quadrotor slung load system, Eng. Sci. Technol. Int. J. 29 (2022) 101038.
[19] R. Puchalski, W. Giernacki, UAV fault detection methods, state-of-the-art, Drones 6 (11) (2022) 330.
[20] J.S. Souza, M.C. Bezerril, M.A. Silva, F.C. Veras, A.C. Lima-Filho, J.G.G. de Souza Ramos, A.V. Brito, Motor speed estimation and failure detection of a small UAV using density of maxima, Frontiers Inf. Technol. Electron. Eng. 22 (7) (2021) 1002–1009.
[21] G.K. Fourlas, G.C. Karras, A survey on fault diagnosis and fault-tolerant control methods for unmanned aerial vehicles, Machines 9 (9) (2021) 197.
[22] K. Guo, W. Zhang, Y. Zhu, J. Jia, X. Yu, Y. Zhang, Safety control for quadrotor UAV against ground effect and blade damage, IEEE Trans. Ind. Electron. 69 (12) (2022) 13373–13383.
[23] N. Ceryan, E.C. Ozkat, N. Korkmaz Can, S. Ceryan, Machine learning models to estimate the elastic modulus of weathered magmatic rocks, Environ. Earth Sci. 80 (12) (2021) 448.
[24] L. Cao, X. Yang, G. Wang, Y. Liu, Y. Hu, Fault detection based on extended state observer and interval observer for UAVs, Aircr. Eng. Aerosp. Technol. 94 (10) (2022) 1759–1771.
[25] H. Hamadi, B. Lussier, I. Fantoni, C. Francis, Data fusion fault tolerant strategy for a quadrotor UAV under sensors and software faults, ISA Trans. 129 (2022) 520–539.
[26] G.K. Fourlas, G.C. Karras, A survey on fault diagnosis and fault-tolerant control methods for unmanned aerial vehicles, Machines 9 (9) (2021) 197.
[27] J. Park, Y. Jung, J.-H. Kim, Multiclass classification fault diagnosis of multirotor UAVs utilizing a deep neural network, Int. J. Control Autom. Syst. 20 (4) (2022) 1316–1326.
[28] O.H. Anidjar, A. Barak, B. Ben-Moshe, E. Hagai, S. Tuvyahu, A stethoscope for drones: Transformers-based methods for UAVs acoustic anomaly detection, IEEE Access 11 (2023) 33336–33353.
[29] X. Zhang, Z. Zhao, Z. Wang, X. Wang, Fault detection and identification method for quadcopter based on airframe vibration signals, Sensors 21 (2) (2021) 581.
[30] M. Saied, B. Lussier, I. Fantoni, H. Shraim, C. Francis, Fault diagnosis and fault-tolerant control of an octorotor UAV using motors speeds measurements, IFAC-PapersOnLine 50 (1) (2017) 5263–5268.
[31] A. Altinors, F. Yol, O. Yaman, A sound based method for fault detection with statistical feature extraction in UAV motors, Appl. Acoust. 183 (2021) 108325.
[32] R. Kılıç, N. Kumbasar, E.A. Oral, I.Y. Ozbek, Drone classification using RF signal based spectral features, Eng. Sci. Technol. Int. J. 28 (2022) 101028.
[33] İ. Yazici, I. Shayea, J. Din, A survey of applications of artificial intelligence and machine learning in future mobile networks-enabled systems, Eng. Sci. Technol. Int. J. 44 (2023) 101455.
[34] E.C. Ozkat, M. Abdioglu, U.K. Ozturk, Machine learning driven optimization and parameter selection of multi-surface HTS maglev, Phys. C: Supercond. Appl. 616 (2024) 1354430.
[35] S. Jeon, J. Kang, J. Kim, H. Cha, Detecting structural anomalies of quadcopter UAVs based on LSTM autoencoder, Pervasive Mob. Comput. 88 (2023) 101736.
[36] H. Lu, Y. Li, S. Mu, D. Wang, H. Kim, S. Serikawa, Motor anomaly detection for unmanned aerial vehicles using reinforcement learning, IEEE Internet Things J. 5 (4) (2017) 2315–2322.
[37] J. Qi, X. Zhao, Z. Jiang, J. Han, An adaptive threshold neural-network scheme for rotorcraft UAV sensor failure diagnosis, in: Advances in Neural Networks–ISNN 2007: 4th International Symposium on Neural Networks, ISNN 2007, Nanjing, China, June 3-7, 2007, Proceedings, Part III 4, Springer, 2007, pp. 589–596.
[38] A. Bondyra, M. Kołodziejczak, R. Kulikowski, W. Giernacki, An acoustic fault detection and isolation system for multirotor UAV, Energies 15 (11) (2022) 3955.
[39] J.-Y. Wu, M. Wu, Z. Chen, X.-L. Li, R. Yan, Degradation-aware remaining useful life prediction with LSTM autoencoder, IEEE Trans. Instrum. Meas. 70 (2021) 1–10.
[40] J.S. Do, A.B. Kareem, J.-W. Hur, Lstm-autoencoder for vibration anomaly detection in vertical carousel storage and retrieval system (vcsrs), Sensors 23 (2) (2023) 1009.